Clustering and alpha-capture reaction rates from first-principle structure calculations for nucleosynthesis

Cite as: AIP Conference Proceedings **2038**, 020013 (2018); https://doi.org/10.1063/1.5078832
Published Online: 13 November 2018

A. C. Dreyfuss, K. D. Launey, J. E. Escher, R. B. Baker, J. P. Draayer, and T. Dytrych

Clustering and Alpha-Capture Reaction Rates from First-Principle Structure Calculations for Nucleosynthesis

A. C. Dreyfuss[1,a)], K. D. Launey[1], J. E. Escher[2], R. B. Baker[1], J. P. Draayer[1] and T. Dytrych[1,3]

[1]*Department of Physics & Astronomy, Louisiana State University, Baton Rouge, LA 70803, USA*
[2]*Lawrence Livermore National Laboratory, Livermore, CA 94550, USA*
[3]*Nuclear Physics Institute, Academy of Sciences of the Czech Republic, 250 68 Řež, Czech Republic*

[a)]Corresponding author: adreyf1@lsu.edu

Abstract. We outline a new formalism that begins with first-principles structure calculations to describe alpha-clustering, and ultimately leads to a description of alpha-capture reaction rates and impacts on abundance patterns from x-ray burst (XRB) nucleosynthesis. We utilize a symmetry-adapted basis, which allows us to extend traditional *ab initio* calculations into the larger model spaces needed for the development of collectivity and clustering in nuclei. In particular, the use of symplectic symmetry allows us to describe spatially expansive states in nuclei – including the Hoyle state of ^{12}C, its 2^+ excitation, and B(E2) transitions – with only one or a few basis configurations. For narrow resonances, coupling to the continuum is weak and the number of competing channels is greatly reduced, so most of the physics of the system is described through the overlap of a wave function for the complete A-particle system, computed with a single symplectic configuration (consisting of several hundreds of basis states), and a cluster basis for a single cluster partitioning. This proves to be a very powerful tool for estimating spectroscopic amplitudes, decay widths, and nuclear reaction rates, with the ability to push toward nuclear reactions involving exotic nuclei that cannot currently be measured. We show preliminary results for the $^{16}\mathrm{O}(\alpha,\gamma)^{20}\mathrm{Ne}$ reaction rate, and consider the implications for abundance patterns determined from XRB nucleosynthesis simulations.

INTRODUCTION

The recent first successful detections of gravitational waves via the Laser Interferometer Gravitational-Wave Observatory (LIGO), together with the Virgo detector near Pisa, and the concurrent observation of gravitational waves and light emission across all wavelengths of a neutron star merger, have opened new ways to further understand astrophysical nucleosynthesis (see [1, 2, 3] and citations therein). These detections have been a major breakthrough in the search for *r*-process (rapid neutron capture) nucleosynthesis sites, and have renewed focus on understanding the nuclear physics that underlies nucleosynthesis, with the aim to improve astrophysics models. Experimental measurements for more exotic systems than ever before achievable are slated to begin within the next few years at the Facility for Rare Isotope Beams (FRIB). In support of these objectives, there is a need for reliable and predictive theoretical frameworks to provide a fuller understanding of these highly unstable systems that play a role in extreme astrophysical environments.

There has been a significant effort in the last decade to develop a fully *ab initio* reaction theory to meet important aspects of this demand for light nuclei (see, e.g., [4, 5, 6]). While these methods provide successful *ab initio* descriptions of reactions, they are computationally costly, especially as heavier systems are considered. We have developed a tool which uses high-quality *ab initio* wave functions to calculate narrow resonance widths, including alpha widths, that can be applied beyond the lightest nuclei. We take advantage of a method for computing overlaps of shell-model and cluster wave functions developed by Suzuki [7] in order to compute spectroscopic amplitudes. The spectroscopic amplitudes are used to compute decay widths based on the *R*-matrix approach, and are supplied as input to reaction rates. We compute spectroscopic amplitudes, decay widths, and reaction rates for the $^{16}\mathrm{O}(\alpha,\gamma)^{20}\mathrm{Ne}$ reaction as a first application of this method.

Proceedings of the 4th International Workshop on "State of the Art in Nuclear Cluster Physics" (SOTANCP4)
AIP Conf. Proc. 2038, 020013-1–020013-6; https://doi.org/10.1063/1.5078832
Published by AIP Publishing. 978-0-7354-1764-9/$30.00

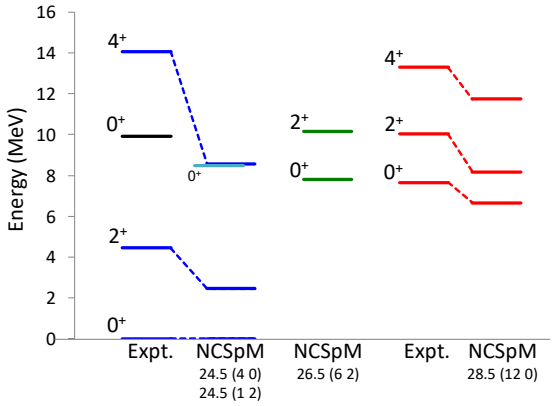

FIGURE 1. Energy spectrum for ^{12}C calculated using the schematic nucleon-nucleon (NN) interaction introduced in [10] within the NCSpM, using four Sp(3, $\mathbb{R}$) irreps: the 0p-0h 24.5(4 0) and 24.5(1 2), 2p-2h 26.5(6 2), and the 4p-4h 28.5(12 0) extended up to $N_{\max} = 20$ ($\hbar\Omega = 18$). Grey arrows indicate $BE(2)$ transition strengths in W.u. NCSpM results are compared to experiment [15, 16]. There are three low-lying excited 0^+ states: the lowest is identified with the experimental Hoyle state (red, right), the second has energy $E_x = 7.8$MeV (green, center), and the third state has energy $E_x = 8.5$ MeV (light blue, left). Figure adapted from [11].

THEORETICAL FRAMEWORK

Emergence of Symmetry Patterns from First Principles

Currently, there are two complementary, symmetry-based no-core shell model approaches which we employ here: the *ab initio* Symmetry-Adapted No-Core Shell Model (SA-NCSM) [8, 9] and the fully microscopic No-Core Symplectic Shell Model (NCSpM) [10, 11]. The SA-NCSM augments the *ab initio* no-core shell model [4, 12] with a symmetry-adapted basis. It is within this framework that an approximate symplectic symmetry naturally emerges from realistic interactions [9]. The NCSpM takes full advantage of this emergent symmetry through use of a symplectic basis, which, for an analytic interaction, can be extended to extremely large model spaces. Both models are briefly described next.

The SA-NCSM is a no-core shell model that uses a realistic NN interaction (e.g., JISP16 [13], and the EM N3LO chiral potential [14]) and a symmetry-adapted basis. In our studies, we employ either an SU(3)-coupled basis or symplectic basis. Basis states are labelled with the deformation-related quantum numbers $(\lambda\,\mu)$, multiplicity κ, and orbital momentum L (in addition to spin degrees of freedom) of the $\mathrm{SU(3)}_{(\lambda\mu)} \overset{\kappa}{\supset} \mathrm{SO(3)}_L$ group chain. An $N_{\max}$ cutoff is introduced, which defines the total number of harmonic oscillator (HO) quanta included in the model space above the minimum quanta for a given nucleus. For a given interaction and $N_{\max}$ cutoff, results using the SA-NCSM are exactly equal to those obtained in the NCSM. The SA-NCSM uses a symmetry-guided scheme to down-select a complete $N_{\max}$ model space to its most physically relevant subspace. This greatly reduces computational cost without the loss of important physics. The SA-NCSM has revealed a remarkable result. Namely, wave functions for light and intermediate-mass nuclei computed within the SA-NCSM reveal a highly-ordered pattern: these first-principles calculations tend to favor large deformation and low spin [9], regardless of the realistic interaction used. This finding is important, as one can use only a few collective basis configurations to capture most of the physics of nuclear low-lying states in the SA-NCSM framework.

The NCSpM is a fully microscopic no-core shell model that takes advantage of these emergent patterns by recognizing that they can be associated with an approximate symmetry, namely, Sp(3, $\mathbb{R}$). In the NCSpM, the model space is organized according to the symplectic Sp(3, $\mathbb{R}$) group [17, 18] and its embedded SU(3) subgroup [19, 20, 21]. This model makes use of a symplectic basis and a simple analytic interaction comprised of symplectic-preserving operators (e.g., the HO potential and the quadrupole moment operator) with one adjustable parameter, in addition to the symplectic-preserving kinetic energy operator. In the same complete $N_{\max}$ model space, results with the same interaction for the NCSpM and NCSM are identical. In contrast to the NCSM, where the model space is divided into $N_{\max}$ subspaces (or horizontal "slices"), the NCSpM organizes the space into irreducible representations of the symplectic group, so-called symplectic "irreps." Symplectic irreps can be viewed as vertical "slices" of the complete model space. Each irrep includes a single shape, also called the "bandhead" [labelled $\sigma = N_\sigma(\lambda_\sigma\mu_\sigma)$], and the

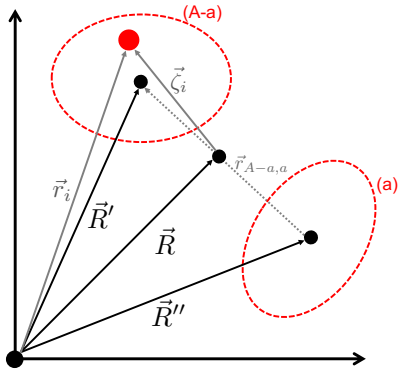

FIGURE 2. Schematic of the A-particle system, partitioned into two clusters comprised of $(A-a)$- and (a)-particles. The position of the i^{th} particle in the space-fixed frame (or lab frame) is $\vec{r}_i$. The center of mass of the A-particle system in the space-fixed frame is $\vec{R}$, while the centers of mass of the $(A-a)$- and (a)-particle clusters are $\vec{R}'$ and $\vec{R}''$, respectively, and the separation between the centers of mass of the two clusters is $\vec{r}_{A-a,a} = \vec{R}' - \vec{R}''$. The set of coordinates $\vec{\zeta}_i = \vec{r}_i - \vec{R}$ are defined relative to the center of mass of the A-particle system. Since $\sum_i \vec{\zeta}_i = 0$, the coordinate $\vec{\zeta}_A$ is linearly dependent on the other relative coordinates.

rotations and vibrations of that shape. Each basis state in a given symplectic irrep, written as $|\sigma n \rho \omega \kappa LM\rangle$, where $n = N_n(\lambda_n \mu_n)$ characterizes the number of excitations above the bandhead. Then $\omega = N_\omega(\lambda_\omega \mu_\omega)$ where $N_\omega = N_n + N_\sigma$ and $\{(\lambda_\sigma \mu_\sigma) \times (\lambda_n \mu_n)\}^{\rho(\lambda_\omega \mu_\omega)}$, with ρ accounting for multiplicity in this coupling. The LM label the angular momentum and its projection, and κ is multiplicity.

The energy spectrum for ^{12}C computed using the NCSpM in a model space consisting of four symplectic irreps extended to $N_{\max} = 20$ agrees remarkably well with experiment (Figure 1). The ground state (gs) rotational band is reproduced by the lowest 0^+, 2^+, and 4^+ states of the two 0p-0h irreps [24.5(4 0) and 24.5(1 2)], although slightly compressed. The lowest 0^+ state of the 4p-4h 28.5(12 0) symplectic irrep coincides with the experimental Hoyle state. The third 0^+ in ^{12}C is reproduced by the lowest 0^+ state of the 2p-2h 26.5(6 2) irrep. The NCSpM also reproduces experimental results for observables which reflect collectivity in the nucleus, such as the $B(E2)$ transition strengths, matter rms radii, as well as electric quadrupole moments, and has been used to study giant monopole and quadrupole resonances in nuclei (see [11]).

Cluster and Symplectic Overlaps

We consider an A-particle system partitioned into two clusters with a and $A-a$ particles (Figure 2). The overlap between the composite A-particle wave function, written in terms of relative coordinates $\vec{\zeta}_i$ with respect to the center of mass (CM) of the A-particle system, $\Psi^{\alpha J^\pi T}_{(A)}(\vec{\zeta}_1 \ldots \vec{\zeta}_{A-1})$, and the cluster wave function written in these same relative coordinates is:

$$u_\nu^{IM_I TM_T}(\vec{r}) = \int d^3\vec{\zeta}_1 \ldots d^3\vec{\zeta}_{A-1} [\Psi^{\alpha J^\pi T}_{(A)}(\vec{\zeta}_1 \ldots \vec{\zeta}_{A-1})]^\dagger \times \mathcal{A}[\{\psi^{\alpha' I'^{\pi'} T'}_{(A-a)}(\vec{\zeta}_1 \ldots \vec{\zeta}_{A-a}) \times \psi^{\alpha'' I''^{\pi''} T''}_{(a)}(\vec{\zeta}_{A-a+1} \ldots \vec{\zeta}_{A-1})\}^{IM_I TM_T} \delta(\vec{r} - \vec{r}_{A-a})] \quad (1)$$

where $\psi^{\alpha' I'^{\pi'} T'}_{(A-a)}$ and $\psi^{\alpha'' I''^{\pi''} T''}_{(a)}$ denote the wave functions for the $(A-a)$- and (a)-particle clusters, respectively. Each cluster carries its own spin, parity ($I'^{\pi'}$ and $I''^{\pi''}$) and isospin (T' and T''). The two clusters are coupled to channel spin I. The α, α', and α'' denote all additional quantum numbers needed to characterize the states, and so we use the channel label $\nu = \{\alpha'\alpha''\alpha; I'^{\pi'} T'; I''^{\pi''} T''\}$. The relative position of the two clusters is denoted with the delta function $\delta(\vec{r} - \vec{r}_{A-a})$, where $\vec{r}_{A-a}$ is the difference in the centers of mass of the two clusters.

The spectroscopic amplitude for this system, which defines the probability to find distinct clusters separated by a distance $\vec{r}$ with relative angular momentum l, is defined as $ru^{J^\pi T}_{\nu l l}(r)$ [22, 23], where:

$$ru^{J^\pi T}_{\nu l l}(r) = r \sum_{M_I m} C^{JM}_{IM_I lm} \int d\hat{r} Y^*_{lm}(\hat{r}) u_\nu^{IM_I TM_T}(\vec{r}). \quad (2)$$

This can be written in terms of an overlap between a NCSpM or SA-NCSM wave function and an SU(3)-coupled cluster wave function: First, by expanding the delta function $\delta(\vec{r} - \vec{r}_{A-a})$ in HO wave functions with the HO constant $b_r = \sqrt{\hbar/\mu\Omega}$, where μ is the reduced mass of the A-particle system. Second, by rewriting the labels α', α'' to reflect explicit dependence on SU(3) quanta and recoupling. And third, by expanding the composite wave function in terms of symplectic basis states, using the brief notation $\omega = (\lambda\,\mu)$:

$$
\begin{aligned}
u^{J^\pi T}_{\nu ll}(r) \;=\; & \sum_n R_{nl}(r) \sum_{\substack{LS\rho\kappa \\ L_0 S_0 \rho_0 \omega_0 \kappa_0}} \sum_{\tilde{n}_0 \tilde{\rho}_0 \tilde{\omega}_0 \tilde{\kappa}_0} c_{\tilde{n}_0 \tilde{\rho}_0 \tilde{\omega}_0 \tilde{\kappa}_0} \Pi_{\substack{LS I' I'' \\ l l L_0 S_0}} \left\{ \begin{array}{ccc} L' & S' & I' \\ L'' & S'' & I'' \\ L & S & I \end{array} \right\} \left\{ \begin{array}{ccc} L & S & J \\ l & 0 & l \\ L_0 & S_0 & J \end{array} \right\} \\
& \times \langle \omega' \kappa' L'; \omega'' \kappa'' L'' \| \omega \kappa L \rangle_\rho \langle \omega \kappa L; (n0) l \| \omega_0 \kappa_0 L_0 \rangle_{\rho_0} \\
& \times \left\langle (A) \tilde{\alpha} \sigma_0 \tilde{n}_0 \tilde{\rho}_0 \tilde{\omega}_0 \tilde{\kappa}_0 (L_0 S_0) J^\pi T | \mathcal{A} \Big\{ \{ |(A-a) \bar{\alpha}' \omega' S' \rangle \times |(a) \bar{\alpha}'' \omega'' S'' \rangle \}^{\rho \omega S} \times |(n0)\rangle \Big\}^{\rho_0 \omega_0 \kappa_0 (L_0 S_0) J^\pi T} \right\rangle \quad (3)
\end{aligned}
$$

where $c_{\tilde{n}_0 \tilde{\rho}_0 \tilde{\omega}_0 \tilde{\kappa}_0}$ is an expansion coefficient and $\Pi_L = \sqrt{2L+1}$; the quantities in the large braces are the SU(2) 9-j symbols for recoupling angular momenta; and the quantities $\langle \omega' \kappa' L'; \omega'' \kappa'' L'' \| \omega \kappa L \rangle_\rho$ and $\langle \omega \kappa L; (n0) l \| \omega_0 \kappa_0 L_0 \rangle_{\rho_0}$ are SU(3) Clebsch-Gordan coefficients, reduced via the Wigner-Eckart theorem with respect to SU(2). The final overlap of Eq. (3) is computed using a recursive formula [7]. The simplicity of this recursion formula hinges on the fact that the symplectic raising operator $A^{(20)}$ acting on the cluster state results in a simple excitation of the relative motion of the two clusters, assuming that both clusters are frozen in their ground states and described by a single symplectic irrep.

The spectroscopic amplitude determines the decay width for a particle with angular momentum l,

$$
\Gamma_l(r_c) = 2 P_l(r_c) \frac{\hbar^2}{2\mu r_c} [r u^{J^\pi T}_{\nu ll}(r)]^2_{r=r_c}. \quad (4)
$$

The penetrability is defined by the Coulomb barrier and depends on the spherical Coulomb-Hankel functions H^+_l as $P_l(r_c) = kr_c / H^+_l(\eta, kr_c)$, where $\eta = Z_1 Z_2 e^2 \mu / \hbar^2 k$ is the Sommerfeld parameter for clusters with charges Z_1 and Z_2, and with $k = \sqrt{2\mu E_\alpha}/\hbar$. Currently, the excitation energy E_α of the excited state with respect to the decay threshold in ^{20}Ne is taken from experiment. The channel radius r_c is typically taken to be a distance at which the nuclear interaction is negligible. For our purposes, the channel radius is taken to be the touching distance of the two clusters ($r_{\rm TD}$), where the radii of the clusters are estimated with an empirical formula $r_c = r_{\rm TD} = 1.1[(A-a)^{1/3} + a^{1/3}]$ fm.

RESULTS AND DISCUSSIONS

We compute the cluster overlap for ^{20}Ne for the ^{16}O + α cluster partition (reaction channel), and consider the ground state 0^+ and first excited 1^- state of ^{20}Ne. The wave functions for these states can be calculated in either *ab initio* SA-NCSM or schematic *NN* NCSpM. We consider both options. For the overlaps, we utilize only one symplectic irrep for each ^{20}Ne state, namely, the most dominant (8 0) (see [24]) for the ground state and (9 0) for 1^-. In addition, only symplectic excitations in the z-directions are considered. Note that the symplectic irrep of the SA-NCSM wave function is estimated approximately from its SU(3) structure.

For the $0^+_{\rm gs}$ state (Figure 3a), we find that the spectroscopic amplitude peaks well within the touching distance ($r_{\rm TD}$ = 4.5 fm) of the two clusters, regardless of which wave function we use for the ^{20}Ne state. For the 1^- state (Figure 3b), results for the SA-NCSM in a full $N_{\rm max} = 5$ model space do not show clear clustering: the spectroscopic amplitude has three peaks of nearly the same size all well within the touching distance of the two clusters. The α decay width for the corresponding 1.3-MeV resonance according to Eq. (4) is $\Gamma_\alpha = 2.9$ eV, compared to an experimentally derived value of $\Gamma_\alpha = 28(3)$ eV [25]. Such a small decay width indicates that the system does not prefer to decay through this channel. Including only those SU(3) configurations into the SA-NCSM model space that correspond to the most deformed symplectic excitations of the (9 0) bandhead, an extension to $N_{\rm max} = 11$ is considered for the 1^- wave function. The result shows a clear identification of two clusters, with the spectroscopic amplitude peaking beyond the touching distance of the two clusters and a decay width of $\Gamma_\alpha = 63$ eV. This suggests that the $N_{\rm max} = 5$ model space is too constricted to allow for cluster development. A NCSpM wave function for the 1^- state, computed using the irrep built on the $\sigma = 49.5(9\,0)$ bandhead within an $N_{\rm max} = 13$ model space, is considered for comparison. This result shows a large peak at the touching distance of the two clusters, indicating the identification of distinct clusters, and a $\Gamma_\alpha = 25$ eV, which agrees with the experimental value.

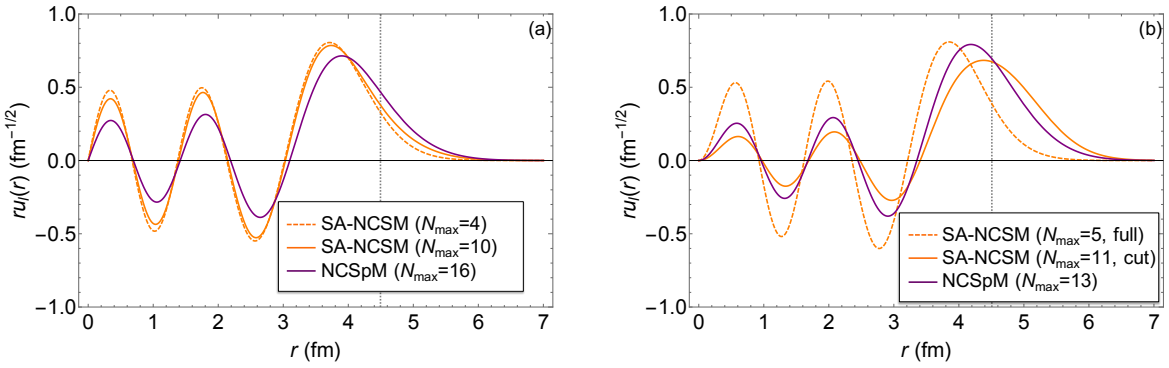

FIGURE 3. (a) Spectroscopic amplitudes for the 0^+_{gs} state of ^{20}Ne considering the $\{^{16}\text{O} + \alpha\}$ cluster partition. The ^{20}Ne wave function is computed using the SA-NCSM in $N_{max} = 4$ (orange, dashed) and $N_{max} = 10$ (orange, solid) model spaces. The NCSpM is used to compute the ^{20}Ne wave function using the $\sigma = 48.5(8\,0)$ irrep extended up to $N_{max} = 16$ (purple, solid). (b) Spectroscopic amplitudes for the first excited 1^- state of ^{20}Ne considering the $\{^{16}\text{O} + \alpha\}$ cluster partition. The SA-NCSM is used to compute the 1^- wave function in a full $N_{max} = 5$ SA-NCSM model space (orange, dashed), and an $N_{max} = 11$ SA-NCSM model space that is down-selected to include only the most deformed basis configurations (orange, solid). An NCSpM wave function for the 1^- state of ^{20}Ne is computed using the $\sigma = 49.5(9\,0)$ irrep extended up to $N_{max} = 13$ (purple, solid). The dotted grey lines indicate the touching distance of the two clusters.

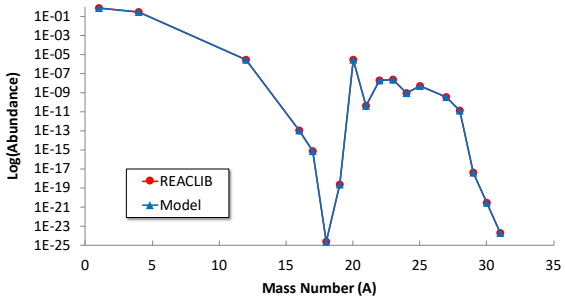

FIGURE 4. Abundance patterns from x-ray burst (XRB) nucleosynthesis simulations, with reaction rates calculated using the NCSpM and the SA-NCSM ("Model"; blue triangles) compared to current REACLIB [28] data ("REACLIB"; red circles), and fixed astrophysical conditions. Abundances are sampled at $t = 1000s$ after the simulated burst begins.

For x-ray burst (XRB) temperatures (1 GK), the Gamow window peaks almost at the energy of the 1^- resonance state, and so this contribution dominates the $^{16}\text{O}(\alpha,\gamma)^{20}\text{Ne}$ reaction rate in XRBs. Using the narrow resonance approximation, we compute the contribution to the $^{16}\text{O}(\alpha,\gamma)^{20}\text{Ne}$ reaction rate through the 1^- resonance, using our calculated alpha-decay widths. These rates are supplied to a simple XRB nucleosynthesis simulation, based on the `Xnet` code [26]. We use a simple nuclear network containing stable nuclei and proton-heavy isotopes with $A \leq 64$ and fixed astrophysical conditions for all simulations. The abundance patterns obtained using the reaction rates calculated from the SA-NCSM wave functions with both model spaces as well as the NCSpM are precisely the same as the abundance pattern produced by using existing experimental data (see Figure 4). This indicates that the XRB nucleosynthesis modeled in this simulation is not sensitive to this reaction rate, despite its role in igniting the (α, p) process [27]. This study opens the path to explore other α-induced reactions for intermediate-mass nuclei, including $\alpha + {}^{15}\text{O}$, which is the focus of work in progress and is expected to have a tremendous impact on XRB nucleosynthesis [28].

Conclusions

We show preliminary results using a new tool for estimating reaction rates using wave functions calculated using the *ab initio* SA-NCSM and the fully microscopic NCSpM. The method is illustrated through calculating spectroscopic

amplitudes for alpha clusters in the 0^+ ground state and the 1^- excited state of ^{20}Ne and by estimating the alpha widths for $^{16}O(\alpha,\gamma)^{20}Ne$ reaction through the 1.3-MeV 1^- resonance. We find evidence of α clustering in the 1^- state, with an enhanced spectroscopic amplitude near the touching distance of the two clusters and a calculated value of $\Gamma_\alpha = 25$ eV, close to experiment. We find that such a small deviation in width has no major impact on abundances of nuclei produced in simple simulations of XRB nucleosynthesis.

ACKNOWLEDGMENTS

This work was supported by the U.S. NSF (OIA-1738287, ACI -1713690), SURA, and the Czech SF (16-16772S), and benefitted from computing resources provided by Blue Waters, LSU (`www.hpc.lsu.edu`), and the National Energy Research Scientific Computing Center (NERSC). Part of this work was performed under the auspices of the DOE by Lawrence Livermore National Laboratory under Contract No. DE-AC52-07NA27344, with support from the U.S. Department of Energy, Office of Science, Office of Workforce Development for Teachers and Scientists, Office of Science Graduate Student Research (SCGSR) program, and from LLNL's LDRD program (16-ERD-022). The SCGSR program is administered by the Oak Ridge Institute for Science and Education (ORISE) for the DOE. ORISE is managed by ORAU under contract number DE-SC0014664.

REFERENCES

[1] B. P. Abbott *et al.*, Phys. Rev. Lett. **119**, p. 161101 (2017).
[2] D. A. Coulter *et al.*, Science **358**, p. 1556 (2017).
[3] B. P. Abbott *et al.*, ApJ **848**, p. L12 (2017).
[4] B. Barrett, P. Navrátil, and J. Vary, Prog. Part. Nucl. Phys. **69**, p. 131 (2013).
[5] A. Calci, P. Navrátil, R. Roth, J. Dohet-Eraly, S. Quaglioni, and G. Hupin, Phys. Rev. Lett. **117**, p. 242501 (2016).
[6] S. Quaglioni, C. Romero-Redondo, P. Navrátil, and G. Hupin, Phys. Rev. C **97**, p. 034332 (2018).
[7] Y. Suzuki, Nucl. Phys. A **448**, p. 395 (1986).
[8] T. Dytrych, K. D. Launey, J. P. Draayer, P. Maris, J. P. Vary, E. Saule, U. Catalyurek, M. Sosonkina, D. Langre, and M. A. Caprio, Phys. Rev. Lett. **111**, p. 252501 (2013).
[9] K. D. Launey, T. Dytrych, and J. P. Draayer, Prog. Part. Nucl. Phys. **89**, p. 101 (2016).
[10] A. C. Dreyfuss, K. D. Launey, T. Dytrych, J. P. Draayer, and C. Bahri, Phys. Lett. B **727**, p. 511 (2013).
[11] A. C. Dreyfuss, K. D. Launey, T. Dytrych, J. P. Draayer, R. B. Baker, C. Deibel, and C. Bahri, Phys. Rev. C **95**, p. 044312 (2017).
[12] P. Navrátil, J. P. Vary, and B. R. Barrett, Phys. Rev. Lett. **84**, p. 5728 (2000).
[13] A. Shirokov, J. Vary, A. Mazur, and T. Weber, Phys. Lett. B **644**, p. 33 (2007).
[14] R. Machleidt, Phys. Rev. C **63**, p. 024001 (2001).
[15] F. Ajzenberg-Selove and J. Kelley, Nucl. Phys. A **506**, p. 1 (1990).
[16] M. Itoh *et al.*, Phys. Rev. C **84**, p. 054308 (2011).
[17] G. Rosensteel and D. J. Rowe, Phys. Rev. Lett. **38**, p. 10 (1977).
[18] D. J. Rowe, Reports on Progr. in Phys. **48**, p. 1419 (1985).
[19] J. P. Elliott, Proc. Roy. Soc. A **245**, p. 128 (1958).
[20] J. P. Elliott, Proc. Roy. Soc. A **245**, p. 562 (1958).
[21] J. P. Elliott and M. Harvey, Proc. Roy. Soc. A **272**, p. 557 (1962).
[22] R. G. Lovas, R. J. Liotta, A. Insolia, K. Varga, and D. S. Delion, Physics Reports **294**, p. 265 (1998).
[23] M. Kimura, Phys. Rev. C **69**, p. 044319 (2004).
[24] G. K. Tobin, M. C. Ferriss, K. D. Launey, T. Dytrych, J. P. Draayer, A. C. Dreyfuss, and C. Bahri, Phys. Rev. C **89**, p. 034312 (2014).
[25] H. Costantini *et al.*, Phys. Rev. C **82**, p. 035802 (2010).
[26] W. Hix and F. K. Thielemann, J. Comput. Appl. Math. **109**, p. 321 (1999).
[27] J. L. Fisker, H. Schatz, and F.-K. Thielemann, ApJS **174**, p. 261 (2008).
[28] R. H. Cyburt *et al.*, ApJS **189**, p. 240 (2010).